Large carbon cycle sensitivities to climate across a permafrost thaw gradient in subarctic Sweden

Kuang-Yu Chang*,
Climate and Ecosystem Sciences Division, Lawrence Berkeley National Laboratory, Berkeley, California, USA
William J. Riley,
Climate and Ecosystem Sciences Division, Lawrence Berkeley National Laboratory, Berkeley, California, USA
Patrick M. Crill,
Department of Geological Sciences, Stockholm University, Stockholm, Sweden
Robert F. Grant,
Department of Renewable Resources, University of Alberta, Edmonton, Alberta, Canada
Virginia I. Rich,
Department of Microbiology, The Ohio State University, Columbus, Ohio, USA
and,
Scott R. Saleska,
Department of Ecology and Evolutionary Biology, University of Arizona, Tucson, Arizona, USA

*Corresponding author: Kuang-Yu Chang, ckychang@lbl.gov
Climate and Ecosystem Sciences Division, Lawrence Berkeley National Laboratory
Berkeley, California, USA

25 Phone: (510) 495-8141

Abstract

Permafrost peatlands store large amounts of carbon potentially vulnerable to decomposition. However, the fate of that carbon in a changing climate remains uncertain in models due to complex interactions among hydrological, biogeochemical, microbial, and plant processes. In this study, we estimated effects of climate forcing biases present in global climate reanalysis products on carbon cycle predictions at a thawing permafrost peatland in subarctic Sweden. The analysis was conducted with a comprehensive biogeochemical model (*ecosys*) across a permafrost thaw gradient encompassing intact permafrost palsa with an ice core and a shallow active layer, partly thawed bog with a deeper active layer and a variable water table, and fen with a water table close to the surface, each with distinct vegetation and microbiota. Using *in situ* observations to correct local cold and wet biases found in the Global Soil Wetness Project Phase 3 (GSWP3) climate reanalysis forcing, we demonstrate good model performance by comparing predicted and observed carbon dioxide (CO_2) and methane (CH_4) exchanges, thaw depth, and water table depth. The simulations driven by the bias-corrected climate suggest that the three peatland types currently accumulate carbon from the atmosphere, although the bog and fen sites can have annual positive radiative forcing impacts due to their higher CH_4 emissions. Our simulations indicate that projected precipitation increases could accelerate CH_4 emissions from the palsa area, even without further degradation of palsa permafrost. The GSWP3 cold and wet biases for this site significantly alter simulation results and lead to erroneous active layer depth (ALD) and carbon budget estimates. Biases in simulated CO_2 and CH_4 exchanges from biased climate forcing are as large as those among the thaw stages themselves at a landscape-scale across the

examined permafrost thaw gradient. Future studies should thus not only focus on changes in carbon budget associated with morphological changes in thawing permafrost, but also recognize the effects of climate forcing uncertainty on carbon cycling.

1. Introduction

Confidence in future climate projections depends on the accuracy of terrestrial carbon budget estimates, which are presently very uncertain (Friedlingstein et al., 2014; Arneth et al., 2017). In addition to the complexity in physical process representations, a major source of this uncertainty comes from challenges in quantifying climate responses induced by biogeochemical feedbacks. Increases in atmospheric carbon dioxide (CO_2) concentrations can directly stimulate carbon sequestration from plant photosynthesis (Cox et al., 2000; Friedlingstein et al., 2006) and indirectly stimulate carbon emissions (e.g., from soil warming and resulting increased respiration), although the predicted magnitudes of these exchanges strongly depend on model process representations (Zaehle et al., 2010; Grant, 2013, 2014; Ghimire et al., 2016; Chang et al, 2018).

The undecomposed carbon stored in permafrost is of critical importance for biogeochemical feedbacks to climate because it is about twice as much as currently is in the atmosphere (Hugelius et al., 2014) and is vulnerable to release to the atmosphere as permafrost thaws (Schuur et al., 2015). O'Donnell et al. (2012) suggested that permafrost thaw would result in a net loss of soil organic carbon from the entire peat column because accumulation rates at the surface were insufficient to balance deep soil organic carbon losses upon thaw. Jones et al. (2017) indicated that the loss of sporadic and discontinuous permafrost by 2100 could result in a release of up to 24 Pg of soil carbon from permafrost peatlands to the atmosphere. Lundin et al. (2016) reported that it is plausible (71% probability) for the high latitude terrestrial landscapes to serve as a net carbon source to the atmosphere, although its peatland components would remain atmospheric carbon sinks.

In addition to the overall carbon balance of the changing Arctic, the type of carbon gaseous emission is important to climate feedbacks. High latitudes are predicted to get wetter (IPCC, 2014), and saturated anaerobic conditions facilitate methane (CH_4) production, which is a much more efficient greenhouse gas than CO_2 in terms of global warming potential. Even habitats that can be net carbon sinks can produce positive radiative forcing impacts on climate due to CH_4 release, as Bäckstrand et al. (2010) showed for a subarctic peatland. Under projected warming and wetting trends in the Arctic (Collins et al., 2013; Bintanja and Andry, 2017), carbon cycle feedbacks over the permafrost region could become stronger as increased precipitation enhances surface permafrost thaw and strengthens CH_4 emissions by expansion of anaerobic volume (Christensen et al., 2004; Wickland et al., 2006).

The Stordalen Mire in northern Sweden (68.20°N, 19.05°E) is in the discontinuous permafrost zone, encompassing a mosaic of thaw stages with associated distinct hydrology and vegetation (Christensen et al. 2004; Malmer et al., 2005), microbiota (Mondav and Woodcroft et al., 2014; Mondav et al., 2017; Woodcroft and Singleton et al., 2018), and organic matter chemistry (Hodgkins et al., 2014). These landscapes have been shifting over the last half-century to a more thawed state, likely due to recent warming (Christensen et al. 2004). Drier hummock sites dominated by shrubs have degraded to wetter sites dominated by graminoids (Malmer et al., 2005; Johansson et al., 2006). The thaw-induced habitat shifts are associated with increases in landscape-scale CH_4 emissions (Christensen et al. 2004; Johansson et al., 2006; Cooper et al., 2017) reflective of the higher CH_4 emissions of the wetter thawed habitats (McCalley et al., 2014). The higher CO_2 uptake in later thaw-stage habitats has not compensated for the

98 increase in positive radiative forcing from elevated CH_4 emissions (Bäckstrand et al.,
99 2010; Deng et al., 2014).
100 The impacts of climate sensitivity on the terrestrial carbon cycle have been
101 investigated at the global scale, and the results highlight the need to consider uncertainty
102 in climate datasets when evaluating permafrost region carbon cycle simulations
103 (Ahlström et al., 2017; Guo et al., 2017; Wu et al., 2017). Ahlström et al. (2017) showed
104 that climate forcing biases are responsible for a considerable fraction (~40%) of the
105 uncertainty range in ecosystem carbon predictions from 18 Earth System Models (ESMs)
106 reported by Anav et al. (2013). Guo et al. (2017) concluded that the differences in climate
107 forcing contribute to significant differences in simulated soil temperature, permafrost
108 area, and Active Layer Depth (ALD). Wu et al. (2017) demonstrated that differences
109 among climate forcing datasets contributes more to predictive uncertainty than
110 differences in apparent model sensitivity to climate forcing. However, notably, none of
111 these studies accessed the effects on CH_4 emissions, and their spatial resolution could not
112 represent site-level spatial heterogeneity observed in arctic tundra (Grant et al. 2017a;
113 2017b).
114 Here, we use the ecosystem model *ecosys*, which employs a comprehensive set of
115 coupled biogeochemical and hydrological processes, to estimate the effects of climate
116 forcing uncertainty and sensitivity on CO_2 and CH_4 exchanges and ALD simulations. For
117 the Stordalen Mire site, we estimated bias in the Global Soil Wetness Project Phase 3
118 (GSWP3) climate reanalysis dataset using site-level long-term meteorological
119 measurements and evaluated impacts on simulated soil and plant processes across the
120 permafrost thaw gradient. This approach enables us to assess model sensitivity to

individual climate forcing biases, instead of the aggregated uncertainty range embedded in climate datasets (e.g., variations of climate conditions represented in different climate datasets) presented in previous studies. We address the following questions for our study site at the Stordalen Mire: (1) What are the biases embedded in the GSWP3 climate reanalysis dataset? (2) How do those biases affect model predictions of ALD, CO_2 exchanges, and CH_4 exchanges? (3) How does climate sensitivity vary across the stages of permafrost thaw? In addition to improving understanding of permafrost responses to climate, we identify ecosystem carbon prediction uncertainty induced by climate forcing uncertainty in general as the biases found in GSWP3 were consistent with other climate reanalysis datasets during the last decade (section 3).

2. Methods and Data

2.1 Study site description

Our study sites are located at the Stordalen Mire (68.20 °N, 19.03 °E: 351 m above sea level), which is about 10 km southeast of the Abisko Scientific Research Station (ANS) in northern Sweden. Significant changes in climate over this region have been recorded during the last few decades. The annual mean air temperature measured at the ANS has risen by 2.5 °C from 1913 to 2006, where it exceeded the 0 °C threshold (0.6 °C in 2006) for the first time over the past century (Callaghan et al., 2010). The measured annual total precipitation has also increased from 306 mm y^{-1} (years 1913 to 2009) to 336 mm y^{-1} (years 1980 to 2009) (Olefeldt and Roulet, 2012), along with increased variability in extreme precipitation (Callaghan et al., 2010). The measured annual maximum snow depth has increased from 59 cm (years 1957 to 1971) to 70 cm

144 (years 1986 to 2000), and the snow cover period with snow depth greater than 20 cm has
145 decreased from 5.8 months (years 1957 to 1971) to 4.9 months (years 1986 to 2000)
146 (Malmer et al., 2005). Inception of peat deposition at the Stordalen Mire has been dated
147 at around 6,000 calendar years before present (cal. BP) (Sonesson 1972) in the southern
148 part of the mire and at around 4,700 cal. BP in the northern part (Kokfelt et al., 2010).
149 Kokfelt et al. (2010) suggested that permafrost aggregation initiated during the Little Ice
150 Age (around 120–400 cal. BP) in the Stordalen Mire.

151 The Stordalen Mire can be broadly classified into three peatland types: intact
152 permafrost palsa, partly thawed bog, and fen (Hodgkins et al., 2014), hereafter referred to
153 as palsa, bog, and fen (Figure 1). The spatial distribution of these peatland types in 2000
154 are described in Olefeldt and Roulet (2012). The palsa sites are ombrotrophic and raised
155 0.5 to 2.0 m above their surroundings, with a relatively thin peat layer (0.4 to 0.7 m,
156 Rydén et al., 1980), thinner active layer depth (less than 0.7 m in late summer), and no
157 measurable water table depth (Bäckstrand et al., 2008a; 2008b; Olefeldt and Roulet,
158 2012). The bog sites are ombrotrophic and are wetter than the palsa sites, with a thicker
159 peat layer (0.5 to ~1 m, Rydén et al., 1980), deeper ALD (greater than 0.9 m), and water
160 table depth fluctuating from 35 cm below the peat surface to the ground surface
161 (Bäckstrand et al., 2008a; 2008b; Olefeldt and Roulet, 2012). The fen sites are
162 minerotrophic, receiving a large amount of water from a lake to the east of the mire, with
163 water table depths near or above the ground surface (Bäckstrand et al., 2008a; 2008b;
164 Olefeldt and Roulet, 2012). All three of the investigated peatland types were there before
165 1930's, based on Swedish military photography.

Differences in hydrology and permafrost conditions create high spatial heterogeneity with different soil moisture, pH, and nutrient conditions that support different plant communities (Bäckstrand et al., 2008a; 2008b). The palsa is dominated by dwarf shrubs with some sedges, feather mosses, and lichens (Malmer et al., 2005; Bäckstrand et al., 2008a; 2008b; Olefeldt and Roulet, 2012). The bog is dominated by *Sphagnum* spp. mosses with a moderate abundance of sedges (Malmer et al., 2005; Bäckstrand et al., 2008a; 2008b; Olefeldt and Roulet, 2012). The fen sites we studied are dominated by sedges (Bäckstrand et al., 2008a; 2008b).

2.2 Field measurements

Continuous daily meteorological measurements have been recorded at the ANS since 1913, including air temperature, precipitation, wind speed, wind direction, relative humidity, and snow depth. Measurements of solar radiation, longwave radiation, and soil temperature are also available at the ANS since 1982. The soil thaw depth (measured to 90 cm) and water table depth measurements were taken in the three peatland types 3 to 5 times per week from early May to mid-October during 2003 to 2007 (Bäckstrand et al., 2008b).

CO_2 and CH_4 exchanges at the three peatland types were measured with automated chambers during the thawed seasons from 2002 to 2007 (Bäckstrand et al., 2008b). Chamber lids were removed when snow accumulates in winter (around November), and the sampling period for each year ranged from days 87–147 in 2002 (shortest) and days 148–341 in 2005 (longest) (Bäckstrand et al., 2008b; Bäckstrand et al., 2010). Three chambers were in the palsa, three were in the bog, and two were in the

189 fen (we term each chamber a 'subsite' in the following). Each chamber covered an area
190 of 0.14 m^2 with a height of 25–45 cm depending on the vegetation and the depth of
191 insertion and was closed for 5 minutes every 3 hours to measure CO_2 and total
192 hydrocarbon (THC) exchanges. CH_4 exchanges were manually observed approximately 3
193 times per week, and these measurements were used to quantify the proportion of CH_4 in
194 the measured THC (Bäckstrand et al., 2008a). The CH_4 exchanges were near zero in the
195 palsa sites (Bäckstrand et al., 2008a; Bäckstrand et al., 2008b; Bäckstrand et al., 2010), so
196 they were not used in model evaluation. We used the CO_2 and CH_4 exchanges observed
197 at 3-hourly steps when the R^2 values recorded in the measurements were greater than 0.8
198 (Tokida et al., 2007), and then calculated the associated daily mean exchanges when there
199 were 8 measurements per day (Table 1). The quality-controlled daily measurements only
200 covered 12.4–33.7% of the daily data points because of the lack of continuous quality-
201 controlled 3-hourly measurements. The data screening was applied to exclude unreliable
202 measurements and avoid biases from inappropriate gap filling, which is necessary for
203 model evaluations. More detailed descriptions of the CO_2 and CH_4 exchanges
204 measurements can be found in Bäckstrand et al. (2008a).
205
206 **2.3 GSWP3**
207 GSWP3 is an ongoing modeling activity that provides global gridded
208 meteorological forcing (0.5° x 0.5° resolution) and investigates changes in energy, water,
209 and carbon cycles throughout the 20th and 21st centuries. The GSWP3 dataset is based on
210 the 20th Century Reanalysis (Compo et al., 2011), using a spectral nudging dynamical
211 downscaling technique described in Yoshimura and Kanamitsu (2008). A more detailed

description of the GSWP can be found in Dirmeyer (2011) and van den Hurk et al. (2016).

In this study, we extracted the meteorological conditions at the Stordalen Mire from 1901 to 2010 from the GSWP3 climate reanalysis dataset. The 3-hourly products of air temperature, precipitation, solar radiation, wind speed, and specific humidity were interpolated to hourly intervals with cubic spline interpolation to serve as the meteorological inputs used in our model.

The GSWP3 dataset was chosen over other existing climate reanalysis datasets for its spatial and temporal resolutions. For example, the Climatic Research Unit (CRU; Harris et al., 2014) dataset provided monthly meteorological forcing at 0.5° x 0.5° resolution; the National Centers for Environmental Prediction (NCEP; Kalnay et al., 1996; Kanamitsu et al., 2002) dataset provided 6-hourly meteorological forcing at T62 Gaussian grid (~1.915° x 1.895° resolution); the CRUNCEP (Viovy, 2018) dataset provided 6-hourly meteorological forcing at 0.5° x 0.5° resolution; and the European Centre for Medium-Range Weather Forecasts (ECMWF; Berrisford et al., 2011) dataset provided 3-hourly meteorological forcing with 125 km (~1.125°) horizontal resolution.

2.4 Model description

Ecosys is a comprehensive biogeochemistry model that simulates ecosystem responses to diverse environmental conditions with explicit representations of microbial dynamics and soil carbon, nitrogen, and phosphorus biogeochemistry. The aboveground processes are represented in multi-layer plant interacting canopies, and the belowground processes are represented in multiple soil layers with multi-phase subsurface reactive

transport. *Ecosys* operates at variable time steps (down to seconds) determined by convergence criteria, and it can be applied at patch-scale (spatially homogenous one-dimensional) and landscape-scale (spatially variable two- or three-dimensional). Detailed descriptions, including inputs, outputs, governing equations, parameters, and references of the *ecosys* model can be found in Grant (2013). A qualitative summery of the *ecosys* model structure is provided in the supplemental material to this article.

The *ecosys* model has been extensively tested against eddy covariance fluxes and related ecophysiological measurements with a wide range of sites and weather conditions in boreal, temperate, and tropical forests (Grant et al., 2007a; Grant et al., 2007c; Grant et al., 2009a; Grant et al., 2009b; Grant et al., 2009c; Grant et al., 2010), wetlands (Dimitrov et al., 2011; Grant et al., 2012b; Dimitrov et al., 2014; Mezbahuddin et al., 2014), grasslands (Grant and Flanagan, 2007; Grant et al., 2012a), tundra (Grant et al., 2003; Grant et al., 2011b; Grant 2015; Grant et al., 2015), croplands (Grant et al., 2007b; Grant et al., 2011a), and other permafrost-associated habitats (Grant and Roulet, 2002; Grant, 2017a; Grant et al., 2017b). All *ecosys* model structures are unchanged from those described in these earlier studies.

2.5 Experimental design

To evaluate the effects of climate on model predictions, we conducted four sets of simulations at each of the three peatland types at the Stordalen Mire from 1901 to 2010. The climate data from 1901 to 2001 were used for model initialization (i.e., spinup) and those from 2002 to 2010 were used for analysis. The 110 year simulations were performed to ensure the simulation was equilibrated with local climate (Grant et al. 2017a).

258 The meteorological conditions for all the simulations were based on the hourly
259 data extracted from the GSWP3 climate reanalysis dataset (section 2.3). The monthly
260 mean bias of the GSWP3 for this location was calculated by comparing it to the air
261 temperature and precipitation measured at the ANS, for years 1913 to 2010 (section 3.1).
262 The full series of air temperature and precipitation extracted from GSWP3 were then
263 bias-corrected using the monthly mean bias calculated from 1913 to 2010; we label this
264 model scenario CTRL. Our bias correction was conceptually similar to the one used in
265 Ahlström et al. (2017), where the bias-corrected climate forcing fields were the ESM
266 outputs adjusted by the corresponding bias calculated from observations in a reference
267 period.
268 The simulation results from CTRL should represent the reliability of applying
269 *ecosys* at the Stordalen Mire because CTRL is driven by the best local climate
270 description. We first evaluated predicted thaw depth, water table depth, and CO_2 and CH_4
271 exchanges using the CTRL simulation (section 3.2 to 3.4). In the second set of
272 simulations, BIASED-COLD, the biased GSWP3 air temperature data was used, and we
273 corrected only the GSWP3 precipitation. Deviations between CTRL and BIASED-COLD
274 reflect biased air temperature's effects on responses across the thaw gradient. In the third
275 set of simulations, BIASED-WET, we bias-corrected the air temperature extracted from
276 GSWP3, which allows us to quantify the effects of biased precipitation. Finally, we used
277 the meteorological conditions directly extracted from GSWP3 to drive our fourth set of
278 simulations, BIASED-COLD&BIASED-WET, which reveals the uncertainty range of
279 subarctic peatland simulation associated with the local biases in GSWP3 climate forcing.

While the three peatland types share the same climate conditions, they differ in soil hydrologic conditions and vegetation characteristics (section 2.1; Figure 1). The bulk density and porosity profiles were set to the values reported in Rydén et al. (1980), who suggested a decreasing trend of bulk density and an increasing trend of porosity from palsa (0.12 Mgm^{-3} at surface; 92–93% within the upper 10 cm) to bog and fen (0.06 Mgm^{-3} at surface; 96–97% within the upper 10 cm). The peatland soil carbon-to-nitrogen (CN) ratios and pH values were assigned according to Hodgkins et al. (2014), who documented an increasing trend of pH from palsa (4.0), to bog (4.2), to fen (5.7), and a decreasing trend of soil organic matter CN ratio from bog (46±18), to palsa (39±24), to fen (19±0.4). Common values of field capacity (0.4) and wilting point (0.15) were used for the three peatland types (Deng et al., 2014). The soil property parameters used in our simulation for the three peatland types are summarized in Supplemental Material Table1.

3 Results and Discussion

3.1 GSWP3 climate comparison to observations

As described in section 2.3, we extracted meteorological conditions at the Stordalen Mire from the GSWP3 climate reanalysis dataset. The closest GSWP3 grid cell was centered at 68.0 °N and19.0 °E, which covers the Stordalen Mire and the ANS. The annual mean air temperature and precipitation calculated at this GSWP3 grid cell were -3.65 °C and 683.88 mm y^{-1}, respectively, for years 1913 to 2010. A cold bias (-3.09 °C) was identified in the GSWP3 annual mean air temperature during the 1913 to 2010 period, although a very high correlation coefficient (r = 0.99) was found when compared with the ANS measurements (Figure 2a). Both time series exhibit an overall warming

303 trend from the early 20th century to the present (0.01°C y^{-1}), with an even larger warming
304 trend from 1980 to 2010 (0.05 °C y^{-1} [ANS] and 0.04 °C y^{-1} [GSWP3]).
305 Similarly, the GSWP3 annual total precipitation data correlates well with ANS
306 measurements (r = 0.80) but has a wet bias of 380 mm y^{-1} between 1913 and 2010
307 (Figure 2b). An increasing trend in annual total precipitation was recorded in both time
308 series from the early 20th century to present (0.47 mm y^{-2} [ANS] and 1.07 mm y^{-2}
309 [GSWP3]), although a decreasing trend was found from 1980 to 2010 (-0.56 mm y^{-2}
310 [ANS] and -2.39 mm y^{-2} [GSWP3]).
311 The seasonal cycle of the GSWP3 monthly mean air temperature also matches
312 that measured at the ANS, with a very high correlation coefficient (r = 0.99; Figure 3a).
313 The underestimation bias and inter-annual variability of GSWP3 air temperature are
314 greater in winter (maximum underestimate in December, at -4.52 °C with inter-annual
315 variability of 3.53 °C) and smaller in summer (minimum underestimate in July, at -1.52
316 °C with inter-annual variability of 1.65 °C), respectively.
317 The magnitude and inter-annual variability of the GSWP3 monthly mean
318 precipitation are comparable between winter and summer, while the ANS measurements
319 exhibit stronger seasonality with lower magnitudes during winter. Despite the differences
320 found in seasonal patterns, a high correlation coefficient (r = 0.64) was found between the
321 monthly mean precipitation extracted from GSWP3 and the ANS measurements. The
322 overestimation of monthly mean precipitation was greatest in December (43.25 mm
323 month^{-1}) and smallest in August (18.75 mm month^{-1}).
324 These comparisons suggest that GSPW3 air temperature and precipitation data
325 reasonably capture measured seasonal and long-term trends over past decades, but are

biased cold and wet compared to observations, especially during winter. Similar cold and wet biases exist in CRUNCEP and ECMWF climate reanalysis datasets during our 2003 to 2007 study period (Supplemental Material Figure 1). The annual mean air temperature and precipitation at the Stordalen Mire for years 2003 to 2007 were -2.49 °C and 795.09 mm y^{-1}; -2.46 °C and 708.60 mm y^{-1}; and -2.28 °C and 765.67 mm y^{-1} in the GSWP3, CRUNCEP, and ECMWF climate reanalysis datasets, respectively.

3.2 Model testing

3.2.1 Thaw depth

We first evaluated *ecosys* against observations using bias-corrected climate forcing (i.e., the CTRL simulation). Predicted thaw depth agrees well with measurements collected from 2003 to 2007 for all examined peatland types (Figure 4), with a correlation coefficient of 0.95, 0.87, and 0.41 at the palsa, bog, and fen, respectively. Both simulations and observations show that the rate of thaw depth deepening in the summer varies with peatland type (i.e., relatively slow, moderate, and rapid in the palsa, bog, and fen, respectively).

Predicted and observed maximum thaw depth (i.e., ALD) in the intact permafrost palsa was between 45 and 60 cm in September. In the partly thawed bog, the simulated thaw depth is slightly shallower than that observed before August. The simulated bog thaw depth becomes greater than 90 cm by the end of August, which matches the time when measured thaw depth reaches its maximum. The thaw depth becomes greater than 90 cm by the end of July in the fen. The patterns of thawing permafrost presented here

348 are consistent with Deng et al. (2014), who simulated the same site using the DNDC
349 model.
350
351 **3.2.2 CO_2 exchanges**
352 The daily Net Ecosystem Exchange (NEE) simulated in the CTRL simulation
353 reasonably captures observed seasonal dynamics from 2003 to 2007 for all the examined
354 peatland types (Figure 5). The simulations and observations generally showed net CO_2
355 uptake (with some episodic CO_2 emissions) during summer and release during winter.
356 The observations and simulations also showed large CO_2 emissions in the palsa site
357 during fall of 2004. Simulated fall CO_2 bursts in the three sites in other years could not be
358 confirmed because of a lack of observations during these periods. Similar to the patterns
359 reported in Raz-Yaseef et al. (2016), some episodic CO_2 emission pulses were simulated
360 as surface ice thaws in spring, but there were no measurements to confirm those events.
361 The correlation coefficients of the simulated and observed daily NEE ranged from 0.58 to
362 0.60, and most of the discrepancies between the simulations and observations were within
363 the ranges of NEE variability measured at different subsites (automated chambers) within
364 the same peatland type.
365 As described in section 2.2, simulated CO_2 exchanges were evaluated for 3-hourly
366 and daily time steps when quality-controlled measurements were available (R^2 values and
367 relative root mean squared errors (RRMSEs) shown in Table 2). Simulated NEE is in
368 reasonable agreement with the 3-hourly NEE measurements with RRMSEs ranging
369 from 8.4 to 19.1%. Model comparisons with observations were generally poorer at daily
370 time steps, although the calculated RRMSEs were comparable to those reported in Deng

et al. (2014). We suspect these differences resulted from uncertainty in determining an accurate observed daily NEE representative of the entire peatland type due to (1) limited daily data points (less than 14% across the study period, Table 1) due to lack of continuous quality-controlled 3-hourly measurements and (2) the large variability of daily NEE ranges measured at different subsites within the same peatland type (Figure 5). Our results thus indicate that NEE is affected by thaw stage (Bäckstrand et al., 2010; Deng et al., 2014) and fine scale spatial heterogeneity of the system. More detailed measurements with higher spatial and temporal resolutions within the same peatland type would be necessary to characterize the effects of this type of heterogeneity.

3.2.3 Water table depth and CH_4 exchanges

Simulated water table depth generally captures observed seasonal patterns measured in the bog and fen sites from 2003 to 2007 (Figure 6a, c). During summer, the predicted bog water table depth fluctuates around the ground surface (-7 to -1 cm), and the predicted water table depth is at or above the ground surface in the fen. Water table depths simulated by *ecosys* are generally higher than measured in the bog, where measured water table depths are often below the ground surface with greater seasonal variability. Simulated fen water table depths have better overall fit to observations, being higher (~5 cm) than measurements in 2003 and 2004, close to measurements in 2005 and 2006, and slightly deeper (~2 cm) than measurements in 2007. These differences in modeled and observed water table depth could be driven by the limitations of our one-dimensional column simulation which inhibits lateral water transport and hinders the variations of water table depth, which is a particular issue in simulating the dynamic

water table of the bog. A multi-dimensional simulation that includes realistic topographic effects could help improve the representation of water table dynamics, and estimates of the measurement uncertainty would help facilitate the assessment of simulation bias.

Simulated and measured daily CH_4 exchanges correlate reasonably well in the bog ($r = 0.49$) and well in the fen ($r = 0.65$) across the study period (Figure 6b, d). Both the simulations and observations have stronger CH_4 emissions during summer with peak emissions in late summer. Some episodic CH_4 emission pulses (Mastepanov et al., 2008) were simulated during shoulder seasons, and the simulated amount of post-growing season CH_4 emissions agrees well with those measured in 2007.

Most of the discrepancies between simulated and observed CH_4 emissions were within the variability of measurements across subsites within the same peatland type. The 3-hourly and daily RRMSEs ranged from 11.1 to 22.3% (Table 2) and the daily RRMSEs were comparable to results presented in Deng et al. (2014). Our results show that model evaluation of CH_4 emissions with finer temporal resolution observations is not necessarily superior to evaluation with coarser temporal resolution, as compared to the NEE counterpart, which could be related to weaker CH_4 emission variability measured across subsites within the same peatland type (Figure 6b, d).

3.3 Variability across the permafrost thaw gradient

Thaw rate and ALD increase along the thaw gradient (i.e., palsa to bog to fen), and landscape variations are generally greater than simulated inter-annual variability (Figure 7a). Maximum carbon uptake also increases along the thaw gradient, and variations across the landscape are comparable with simulated intra-seasonal and inter-

417 annual variabilities (Figure 7b). The simulated mean seasonal cumulative NEE were
418 calculated based on the seasonality identified in Bäckstrand et al. (2010), and the results
419 show that the magnitude of mean growing season CO_2 uptake is highest in the fen and
420 lowest in the palsa (Table 3). The same rank applies to the magnitude of mean CO_2
421 emissions over the non-growing season, although differences across the thaw gradient are
422 smaller.

423 CH_4 emission rates increase significantly along the thaw gradient, and the palsa
424 site emissions are negligible (Figure 7c). Mean cumulative CH_4 emissions simulated in
425 the fen are much higher than those in the bog, and most CH_4 emissions occur during the
426 growing season (Table 3). The higher CH_4 emissions in the fen can be attributed to its
427 faster seasonal thaw rate (Figure 7a) and a water table depth close to the surface (Figure
428 6c). Seasonal cumulative NEE and CH_4 emissions from observations could not be
429 accessed due to the lack of continuous quality controlled carbon flux measurements
430 during our study period (Table 1).

431

432 **4. Climate sensitivity of permafrost thaw**

433 **4.1 Thaw responses to climate**

434 For each of the four sets of simulations with different climate forcing (section
435 2.5), simulated mean ALD from 2003 to 2007 is always greatest in the fen and lowest in
436 the palsa (Figure 8). This consistent trend along the thaw gradient indicates that ALDs
437 are largely regulated by their distinct ecological and hydrological conditions, because all
438 three sites had the same climate forcing in each set of simulations (i.e., CTRL, BIASED-
439 COLD, BIASED-WET, and BIASED-COLD&BIASED-WET). Therefore, the palsa,

bog, and fen have different resilience against the changes in climate forcing, and this type of ecosystem resilience plays an important role in determining ALD under changes in climate conditions.

Effects of climate on simulated ALD are similar across peatland types (Figure 8). With increased precipitation (BIASED-WET vs. CTRL), simulated ALD generally becomes deeper with greater inter-annual variability because the increased snowpack depth keeps the soil warmer with lower soil ice content during winter. This effect is less prominent in the comparison between experiments BIASED-COLD and BIASED-COLD&BIASED-WET, because the cold biases in these two experiments (section 3.1) constrain ALD development. For example, summertime soil heating in some of the simulation years was not strong enough to thaw the soil ice between 20-40 cm completely in the BIASED-COLD&BIASED-WET run, resulting in shallower ALDs simulated in the palsa and fen even with the snowpack warming effect. The simulated ALD also becomes deeper with higher air temperature (CTRL vs. BIASED-COLD; BIASED-WET vs. BIASED-COLD&BIASED-WET) at all the examined peatland types. This response is more evident in the comparison between experiments BIASED-WET and BIASED-COLD&BIASED-WET, probably driven by their wet biases (section 3.1) that facilitate ALD deepening (via increased thermal conductivity and advective heat transport; Grant et al. 2017a). Similar dependencies between ALD and climate were shown in Åkerman and Johansson (2008) and Johansson et al. (2013), based on multi-year measurements and snow manipulation experiments.

Therefore, the combined cold and wet biases in the GSWP3 climate reanalysis dataset could counteract their individual effects on simulated ALD development at the

463 Stordalen Mire. Our results indicate a 28.6%, 0.7%, and 11.7% underestimation of ALD
464 simulated in the palsa, bog, and fen, respectively, when applying the GSWP3 climate
465 reanalysis data over this region without proper bias correction (BIASED-
466 COLD&BIASED-WET vs. CTRL). Our sensitivity analysis suggests that projected
467 warming and wetting trends (Collins et al., 2013) could significantly increase ALD in the
468 Arctic, since increases in precipitation and air temperature can both contribute to ALD
469 deepening.
470
471 **4.2 Carbon budget responses to climate**
472 Simulations with the four climate forcing datasets (section 2.5) indicate annual
473 mean (from 2003 to 2007) CO_2 sinks and CH_4 sources, except the weak CO_2 emissions
474 simulated in the fen in experiment BIASED-COLD&BIASED-WET due to reduced
475 sedge productivity driven by increased temperature and oxygen stresses (Figure 9a,b).
476 Our results also indicate that differences in annual CO_2 and CH_4 exchanges across the
477 four climate forcing datasets for a single peatland type are as large as those across
478 peatland types for a single climate forcing dataset (Figure 9a,b). These large CO_2 and
479 CH_4 exchanges climate sensitivities demonstrate that the peatland's dynamical responses
480 to climate have stronger effects on the carbon cycle than on ALDs (Figure 8).
481 With bias-corrected precipitation, increased air temperature (CTRL vs. BIASED-
482 COLD) leads to stronger CO_2 uptake and greater CH_4 emissions at all the examined
483 peatland types (Figure 9a,b), mainly because enhanced sedge growth facilitates carbon
484 cycling under a warmer environment (results not shown). This air temperature sensitivity
485 affects CO_2 and CH_4 exchanges within the same peatland type without significantly

changing ALD (Figure 8). For both experiments, CO_2 uptake and CH_4 emissions are greatest in the fen and lowest in the palsa, consistent with the measurements reported in Bäckstrand et al. (2010) for the same period. Based on the Coupled Model Intercomparison Project, phase 5 (CMIP5) ESM simulations, arctic annual mean surface air temperature is projected to increase by 8.5±2.1 °C over the 21st century (Bintanja and Andry, 2017). This projected air temperature increase is more than double the air temperature difference between site-observed and GSWP3 temperatures, which could significantly enhance CH_4 emissions regardless of palsa degradation into bog and fen.

On the other hand, wet biases (BIASED-WET and BIASED-COLD&BIASED-WET) increase CH_4 emissions in the palsa; wetter and colder conditions result in as much CH_4 release as the current fen, while wetter conditions alone drive palsa emissions comparable to the current bog (Figure 9b). The large precipitation sensitivity found in palsa CH_4 emissions could have strong effects on palsa carbon cycling because arctic precipitation is projected to increase by 50 – 60% towards the end of the 21st century (based on CMIP5 estimates; Bintanja and Andry, 2017). The comparison between experiments BIASED-WET and BIASED-COLD&BIASED-WET shows that in the palsa, increased air temperature strengthens CO_2 uptake and weakens CH_4 emissions. This shift is primarily driven in the model by increased shrub and moss productivity under the warmer environment, which facilitate CO_2 uptake while drying out the soil and reducing CH_4 emissions (results not shown). In the bog and fen sites, increased air temperature under wet bias strengthens both the simulated CO_2 uptake and CH_4 emissions (BIASED-WET vs. BIASED-COLD&BIASED-WET), due to enhanced sedge growth under the warmer environment that facilitates carbon cycling in the experiment

509 BIASED-WET. The low CH_4 emissions in bog and fen simulated in experiment
510 BIASED-COLD&BIASED-WET are driven by increased temperature and oxygen
511 stresses that greatly reduce heterotrophic respiration (CH_4 production) and sedge cover
512 (aerenchyma transport).

513 We assessed the integrated effects of the changes in CO_2 and CH_4 exchanges
514 identified in the full suite of simulations in terms of the Net Carbon Balance (NCB) and
515 net emissions of greenhouse gases expressed as CO_2 equivalents (Net Greenhouse Gas
516 Balance; NGGB). NCB was defined as the sum of the annual total CO_2 and CH_4
517 exchanges. NGGB was defined in a similar fashion as the NCB, but considers the greater
518 radiative forcing potential of CH_4 than CO_2 (28 times over a 100-year horizon, Myhre et
519 al., 2013) when calculating the annual total. The calculated NCB values are mostly
520 negative because the stronger CO_2 uptake dominates the weaker CH_4 emissions (Figure
521 9c). The results suggest that all the examined peatland types serve as net carbon sinks
522 under current climate (CTRL), consistent with the estimates reported in Deng et al.
523 (2014) and Lundin et al. (2016). We find a 24, 36, and 38 g C m^{-2} y^{-1} underestimation of
524 NCB simulated in the palsa, bog, and fen sites, respectively, due to the cold and wet
525 biases in the GSWP3 climate reanalysis dataset (BIASED-COLD&BIASED-WET vs.
526 CTRL). NGGB is affected more strongly by CH_4 emissions (Figure 9d) due to its larger
527 radiative forcing potential. NGGB values are positive over the bog and fen, suggesting
528 that these sites have positive radiative forcing impacts despite being net carbon sinks.
529 NGGB simulated in the palsa is generally negative (i.e., a net sink from the atmosphere)
530 due to lower CH_4 emissions, except for the simulation conducted without any climate bias
531 correction (correcting only air temperature increased CH_4 emissions but not enough to

compensate for the significantly higher CO_2 sink). Our results indicate that the simulated NGGB would be biased by 298, -66, and -252 g CO_2-eq m^{-2} y^{-1} in the palsa, bog, and fen, respectively, without proper bias correction for the GSWP3 climate reanalysis dataset (BIASED-COLD&BIASED-WET vs. CTRL). Using the GSWP3 products directly thus effectively eliminates the positive radiative forcing from the expanding bog and fen, while creating a potentially dramatically inaccurate positive radiative forcing from the shrinking palsa.

4.3 Climate sensitivity versus landscape heterogeneity

Climate sensitivity and landscape heterogeneity are defined here as variability across the four climate forcing datasets for a single peatland type, and variability across three peatland types with bias-corrected climate (CTRL), respectively. We estimated carbon cycle variability associated with climate sensitivity and landscape heterogeneity to quantify the corresponding uncertainty in our annual carbon cycle assessments from 2003 to 2007. Our results indicate that differences in simulated annual mean CO_2 exchanges and NCB from climate sensitivity are greater than those from landscape heterogeneity (Figure 9a,c); i.e., annual CO_2 uptake strength is more sensitive to climate forcing uncertainty than to peatland type representation. In terms of the simulated annual mean CH_4 emissions and NGGB, our results indicate that variability from climate sensitivity is comparable to those from landscape heterogeneity (Figure 9b,d). Therefore, bias-corrected climate and realistic peatland characterization are both necessary to reduce the uncertainty in representing carbon cycling dynamics and their radiative forcing effects.

554 In addition to their effects on carbon cycle predictions, changes in climate
555 conditions also affect permafrost degradation and thus induce changes in areal cover of
556 peatland types. Malmer et al. (2005) showed that there were -0.95, 0.24, and 0.62 ha areal
557 cover changes (-10.3%, 4.0%, and 46.3% percentage changes) from 1970 to 2000 in
558 palsa, bog, and fen, respectively, at the Stordalen Mire. By applying the annual mean
559 CO_2 and CH_4 exchanges simulated with bias-corrected climate from 2003 to 2007, the
560 areal cover changes from 1970 to 2000 alone would lead to -44 kg C y^{-1}, 76 kg C y^{-1}, and
561 2076 kg CO_2-eq y^{-1} changes in annual mean CO_2 exchanges, CH_4 exchanges, and NGGB,
562 respectively, at the Stordalen Mire. The changes in landscape-scale carbon cycle
563 dynamics indicate that the radiative warming impact of increased CH_4 emissions is large
564 enough to offset the radiative cooling impact of increased CO_2 uptake at the Stordalen
565 Mire, consistent with the estimates reported in Deng et al. (2014). The areal cover
566 changes across peatland types could persist or accelerate under the projected warming
567 and wetting trends in the Arctic (Collins et al., 2013; Bintanja and Andry, 2017), which
568 could stimulate CH_4 emissions and produce a stronger radiative warming impact.
569
570 **5. Conclusions**
571 We evaluated the climate bias in a widely used atmospheric reanalysis product
572 (GSWP3) at our northern Sweden Stordalen Mire site. We then applied a comprehensive
573 biogeochemistry model, *ecosys*, to estimate the effects of these biases on active layer
574 development and carbon cycling across a thaw gradient at the site. Our results show that
575 *ecosys* reasonably represented measured hydrological, thermal, and biogeochemical cycle
576 processes in the intact permafrost palsa, partly thawed bog, and fen. We found that the

577 cold and wet biases in the GSWP3 climate reanalysis dataset significantly alter model
578 simulations, leading to biases in simulated Active Layer Depths, Net Carbon Balance,
579 and Net Greenhouse Gas Balance by up to 28.6%, 38 g C m^{-2} y^{-1}, and 298 g CO_2-eq m^{-2}
580 y^{-1}, respectively. The Net Carbon Balance simulated with bias-corrected climate suggests
581 that all the examined peatland types are currently net carbon sinks from the atmosphere,
582 although the bog and fen sites can have positive radiative forcing impacts due to their
583 higher CH_4 emissions.

584 Our results indicate that the annual means of ALD, CO_2 uptake, and CH_4
585 emissions generally increase along the permafrost thaw gradient at the Stordalen Mire
586 under current climate, consistent with previous studies in this region. Our analysis
587 suggests that palsa, bog, and fen differ strongly in their carbon cycling dynamics and
588 have different responses to climate forcing biases. Differences in simulated CO_2 and CH_4
589 exchanges driven by uncertainty from climate forcing are as large as those from
590 landscape heterogeneity across the examined permafrost thaw gradient. Model
591 simulations demonstrate that the palsa site exhibits the strongest sensitivity to biases in
592 air temperature and precipitation. The wet bias in GSWP3 could erroneously increase
593 predicted CH_4 emissions from the palsa site to a magnitude comparable to emissions
594 currently measured in the bog and fen sites. These results also show that increased
595 precipitation projected for high latitude regions could strongly accelerate CH_4 emissions
596 from the palsa area, even without degradation of palsa into bog and fen. Future studies
597 should thus recognize the effects of climate forcing uncertainty on carbon cycling, in
598 addition to tracking changes in carbon budgets associated with areal changes in
599 permafrost degradation.

Acknowledgements

This study was funded by the Genomic Science Program of the United States Department of Energy Office of Biological and Environmental Research under the ISOGENIE project, grant DE-SC0016440, to Lawrence Berkeley Laboratory under contract DE-AC02-05CH11231, and by support from the Swedish Research Council (VR) to PMC. We thank the Abisko Scientific Research Station of the Swedish Polar Research Secretariat for providing the meteorological data.

References

Ahlström, A., Schurgers, G. and Smith, B.: The large influence of climate model bias on terrestrial carbon cycle simulations, Environmental Research Letters, 12(1), 014004, doi:10.1088/1748-9326/12/1/014004, 2017.

Anav, A., Friedlingstein, P., Kidston, M., Bopp, L., Ciais, P., Cox, P., Jones, C., Jung, M., Myneni, R. and Zhu, Z.: Evaluating the Land and Ocean Components of the Global Carbon Cycle in the CMIP5 Earth System Models, J. Climate, 26(18), 6801–6843, doi:10.1175/JCLI-D-12-00417.1, 2013.

Arneth, A., Sitch, S., Pongratz, J., Stocker, B. D., Ciais, P., Poulter, B., Bayer, A. D., Bondeau, A., Calle, L., Chini, L. P., Gasser, T., Fader, M., Friedlingstein, P., Kato, E., Li, W., Lindeskog, M., Nabel, J. E. M. S., Pugh, T. A. M., Robertson, E., Viovy, N., Yue, C. and Zaehle, S.: Historical carbon dioxide emissions caused by land-use changes are possibly larger than assumed, Nature Geoscience, 10(2), 79–84, doi:10.1038/ngeo2882, 2017.

Bäckstrand, K., Crill, P. M., Mastepanov, M., Christensen, T. R. and Bastviken, D.: Non-methane volatile organic compound flux from a subarctic mire in Northern Sweden, Tellus B, 60(2), 226–237, doi:10.1111/j.1600-0889.2007.00331.x, 2008a.

Bäckstrand, K., Crill, P. M., Mastepanov, M., Christensen, T. R. and Bastviken, D.: Total hydrocarbon flux dynamics at a subarctic mire in northern Sweden, Journal of Geophysical Research: Biogeosciences, 113(G3), doi:10.1029/2008JG000703, 2008b.

631 Backstrand, K., Crill, P. M., ski, M. J.-K., Mastepanov, M., Christensen, T. R. and
632 Bastviken, D.: Annual carbon gas budget for a subarctic peatland, Northern
633 Sweden, 14, 2010.
634 Berrisford, P., Dee, D. P., Poli, P., Brugge, R., Fielding, K., Fuentes, M., Kållberg, P. W.,
635 Kobayashi, S., Uppala, S. and Simmons, A.: The ERA-Interim archive Version
636 2.0, 2011.
637 Bintanja, R. and Andry, O.: Towards a rain-dominated Arctic, Nature Climate Change,
638 7(4), 263–267, doi:10.1038/nclimate3240, 2017.
639 Callaghan, T. V., Bergholm, F., Christensen, T. R., Jonasson, C., Kokfelt, U. and
640 Johansson, M.: A new climate era in the sub-Arctic: Accelerating climate changes
641 and multiple impacts, Geophysical Research Letters, 37(14),
642 doi:10.1029/2009GL042064, 2010.
643 Chang, K.-Y., Paw U, K. T. and Chen, S.-H.: The importance of carbon-nitrogen
644 biogeochemistry on water vapor and carbon fluxes as elucidated by a multiple
645 canopy layer higher order closure land surface model, Agricultural and Forest
646 Meteorology, 259, 60–74, doi:10.1016/j.agrformet.2018.04.009, 2018.
647 Christensen, T. R., Johansson, T., Åkerman, H. J., Mastepanov, M., Malmer, N., Friborg,
648 T., Crill, P. and Svensson, B. H.: Thawing sub-arctic permafrost: Effects on
649 vegetation and methane emissions, Geophysical Research Letters, 31(4),
650 doi:10.1029/2003GL018680, 2004.
651 Collins, M., R. Knutti, J. Arblaster, J.-L. Dufresne, T. Fichefet, P. Friedlingstein, X. Gao,
652 W.J. Gutowski, T. Johns, G. Krinner, M. Shongwe, C. Tebaldi, A.J. Weaver and
653 M. Wehner, 2013: Long-term Climate Change: Projections, Commitments and

654 Irreversibility. Climate Change 2013: The Physical Science Basis. Contribution of
655 Working Group I to the Fifth Assessment Report of the Intergovernmental Panel
656 on Climate Change. T. F. Stocker et al., Eds., Cambridge University Press, 1029-
657 1136.
658 Compo, G. P., Whitaker, J. S., Sardeshmukh, P. D., Matsui, N., Allan, R. J., Yin, X.,
659 Gleason, B. E., Vose, R. S., Rutledge, G., Bessemoulin, P., Brönnimann, S.,
660 Brunet, M., Crouthamel, R. I., Grant, A. N., Groisman, P. Y., Jones, P. D., Kruk,
661 M. C., Kruger, A. C., Marshall, G. J., Maugeri, M., Mok, H. Y., Nordli, Ø., Ross,
662 T. F., Trigo, R. M., Wang, X. L., Woodruff, S. D. and Worley, S. J.: The
663 Twentieth Century Reanalysis Project, Quarterly Journal of the Royal
664 Meteorological Society, 137(654), 1–28, doi:10.1002/qj.776, 2011.
665 Cooper, M. D. A., Estop-Aragonés, C., Fisher, J. P., Thierry, A., Garnett, M. H.,
666 Charman, D. J., Murton, J. B., Phoenix, G. K., Treharne, R., Kokelj, S. V., Wolfe,
667 S. A., Lewkowicz, A. G., Williams, M. and Hartley, I. P.: Limited contribution of
668 permafrost carbon to methane release from thawing peatlands, Nature Climate
669 Change, 7(7), 507–511, doi:10.1038/nclimate3328, 2017.
670 Cox, P. M., Betts, R. A., Jones, C. D., Spall, S. A. and Totterdell, I. J.: Acceleration of
671 global warming due to carbon-cycle feedbacks in a coupled climate model, 408,
672 4, 2000.
673 Deng, J., Li, C., Frolking, S., Zhang, Y., Bäckstrand, K. and Crill, P.: Assessing effects of
674 permafrost thaw on C fluxes based on multiyear modeling across a permafrost
675 thaw gradient at Stordalen, Sweden, Biogeosciences, 11(17), 4753–4770,
676 doi:10.5194/bg-11-4753-2014, 2014.

677 Dimitrov, D. D., Bhatti, J. S. and Grant, R. F.: The transition zones (ecotone) between
678 boreal forests and peatlands: Ecological controls on ecosystem productivity along
679 a transition zone between upland black spruce forest and a poor forested fen in
680 central Saskatchewan, Ecological Modelling, 291, 96–108,
681 doi:10.1016/j.ecolmodel.2014.07.020, 2014.
682 Dimitrov Dimitre D., Grant Robert F., Lafleur Peter M. and Humphreys Elyn R.:
683 Modeling the effects of hydrology on gross primary productivity and net
684 ecosystem productivity at Mer Bleue bog, Journal of Geophysical Research:
685 Biogeosciences, 116(G4), doi:10.1029/2010JG001586, 2011.
686 Dirmeyer, P. A.: A History and Review of the Global Soil Wetness Project (GSWP),
687 Journal of Hydrometeorology, 12(5), 729–749, doi:10.1175/JHM-D-10-05010.1,
688 2011.
689 Friedlingstein, P., Cox, P., Betts, R., Bopp, L., von Bloh, W., Brovkin, V., Cadule, P.,
690 Doney, S., Eby, M., Fung, I., Bala, G., John, J., Jones, C., Joos, F., Kato, T.,
691 Kawamiya, M., Knorr, W., Lindsay, K., Matthews, H. D., Raddatz, T., Rayner, P.,
692 Reick, C., Roeckner, E., Schnitzler, K.-G., Schnur, R., Strassmann, K., Weaver,
693 A. J., Yoshikawa, C. and Zeng, N.: Climate–Carbon Cycle Feedback Analysis:
694 Results from the C ^{4} MIP Model Intercomparison, Journal of Climate, 19(14),
695 3337–3353, doi:10.1175/JCLI3800.1, 2006.
696 Friedlingstein, P., Meinshausen, M., Arora, V. K., Jones, C. D., Anav, A., Liddicoat, S.
697 K. and Knutti, R.: Uncertainties in CMIP5 Climate Projections due to Carbon
698 Cycle Feedbacks, Journal of Climate, 27(2), 511–526, doi:10.1175/JCLI-D-12-
699 00579.1, 2014.

Ghimire, B., Riley, W. J., Koven, C. D., Mu, M. and Randerson, J. T.: Representing leaf and root physiological traits in CLM improves global carbon and nitrogen cycling predictions, Journal of Advances in Modeling Earth Systems, 8(2), 598–613, doi:10.1002/2015MS000538, 2016.

Grant, R. F.: Modelling changes in nitrogen cycling to sustain increases in forest productivity under elevated atmospheric CO2 and contrasting site conditions, Biogeosciences, 10(11), 7703–7721, doi:10.5194/bg-10-7703-2013, 2013.

Grant, R. F.: Nitrogen mineralization drives the response of forest productivity to soil warming: Modelling in ecosys vs. measurements from the Harvard soil heating experiment, Ecological Modelling, 288, 38–46, doi:10.1016/j.ecolmodel.2014.05.015, 2014.

Grant R. F. and Flanagan L. B.: Modeling stomatal and nonstomatal effects of water deficits on CO2 fixation in a semiarid grassland, Journal of Geophysical Research: Biogeosciences, 112(G3), doi:10.1029/2006JG000302, 2007.

Grant, R. F. and Roulet, N. T.: Methane efflux from boreal wetlands: Theory and testing of the ecosystem model Ecosys with chamber and tower flux measurements, Global Biogeochemical Cycles, 16(4), 2-1-2–16, doi:10.1029/2001GB001702, 2002.

Grant, R. F., Oechel, W. C. and Ping, C.-L.: Modelling carbon balances of coastal arctic tundra under changing climate, Global Change Biology, 9(1), 16–36, doi:10.1046/j.1365-2486.2003.00549.x, 2003.

Grant, R. F., Black, T. A., Humphreys, E. R. and Morgenstern, K.: Changes in net ecosystem productivity with forest age following clearcutting of a coastal

723 Douglas-fir forest: testing a mathematical model with eddy covariance
724 measurements along a forest chronosequence, Tree Physiol., 27(1), 115–131,
725 2007a.
726 Grant, R. F., Arkebauer, T. J., Dobermann, A., Hubbard, K. G., Schimelfenig, T. T.,
727 Suyker, A. E., Verma, S. B. and Walters, D. T.: Net Biome Productivity of
728 Irrigated and Rainfed Maize–Soybean Rotations: Modeling vs. Measurements,
729 Agronomy Journal, 99(6), 1404, doi:10.2134/agronj2006.0308, 2007b.
730 Grant, R. F., Barr, A. G., Black, T. A., Gaumont□Guay, D., Iwashita, H., Kidson, J.,
731 McCAUGHEY, H., Morgenstern, K., Murayama, S., Nesic, Z., Saigusa, N.,
732 Shashkov, A. and Zha, T.: Net ecosystem productivity of boreal jack pine stands
733 regenerating from clearcutting under current and future climates, Global Change
734 Biology, 13(7), 1423–1440, doi:10.1111/j.1365-2486.2007.01363.x, 2007c.
735 Grant, R. F., Margolis, H. A., Barr, A. G., Black, T. A., Dunn, A. L., Bernier, P. Y. and
736 Bergeron, O.: Changes in net ecosystem productivity of boreal black spruce
737 stands in response to changes in temperature at diurnal and seasonal time scales,
738 Tree Physiology, 29(1), 1–17, doi:10.1093/treephys/tpn004, 2009a.
739 Grant, R. F., Barr, A. G., Black, T. A., Margolis, H. A., Dunn, A. L., Metsaranta, J.,
740 Wang, S., McCaughey, J. H. and Bourque, C. A.: Interannual variation in net
741 ecosystem productivity of Canadian forests as affected by regional weather
742 patterns – A Fluxnet-Canada synthesis, Agricultural and Forest Meteorology,
743 149(11), 2022–2039, doi:10.1016/j.agrformet.2009.07.010, 2009b.
744 Grant, R. F., Hutyra, L. R., Oliveira, R. C., Munger, J. W., Saleska, S. R. and Wofsy, S.
745 C.: Modeling the carbon balance of Amazonian rain forests: resolving ecological

controls on net ecosystem productivity, Ecological Monographs, 79(3), 445–463, doi:10.1890/08-0074.1, 2009c.

Grant, R. F., Barr, A. G., Black, T. A., Margolis, H. A., Mccaughey, J. H. and Trofymow, J. A.: Net ecosystem productivity of temperate and boreal forests after clearcutting—a Fluxnet-Canada measurement and modelling synthesis, Tellus B: Chemical and Physical Meteorology, 62(5), 475–496, doi:10.1111/j.1600-0889.2010.00500.x, 2010.

Grant, R. F., Kimball, B. A., Conley, M. M., White, J. W., Wall, G. W. and Ottman, M. J.: Controlled Warming Effects on Wheat Growth and Yield: Field Measurements and Modeling, Agronomy Journal, 103(6), 1742–1754, doi:10.2134/agronj2011.0158, 2011a.

Grant, R. F., Humphreys, E. R., Lafleur, P. M. and Dimitrov, D. D.: Ecological controls on net ecosystem productivity of a mesic arctic tundra under current and future climates, Journal of Geophysical Research: Biogeosciences, 116(G1), doi:10.1029/2010JG001555, 2011b.

Grant, R. F., Baldocchi, D. D. and Ma, S.: Ecological controls on net ecosystem productivity of a seasonally dry annual grassland under current and future climates: Modelling with ecosys, Agricultural and Forest Meteorology, 152, 189–200, doi:10.1016/j.agrformet.2011.09.012, 2012a.

Grant, R. F., Desai, A. R. and Sulman, B. N.: Modelling contrasting responses of wetland productivity to changes in water table depth, Biogeosciences, 9(11), 4215–4231, doi:10.5194/bg-9-4215-2012, 2012b.

768 Grant R. F., Humphreys E. R. and Lafleur P. M.: Ecosystem CO2 and CH4 exchange in a
769 mixed tundra and a fen within a hydrologically diverse Arctic landscape: 1.
770 Modeling versus measurements, Journal of Geophysical Research:
771 Biogeosciences, 120(7), 1366–1387, doi:10.1002/2014JG002888, 2015.
772 Grant, R. F., Mekonnen, Z. A., Riley, W. J., Wainwright, H. M., Graham, D. and Torn,
773 M. S.: Mathematical Modelling of Arctic Polygonal Tundra with Ecosys: 1.
774 Microtopography Determines How Active Layer Depths Respond to Changes in
775 Temperature and Precipitation, Journal of Geophysical Research: Biogeosciences,
776 122(12), 3161–3173, doi:10.1002/2017JG004035, 2017a.
777 Grant, R. F., Mekonnen, Z. A., Riley, W. J., Arora, B. and Torn, M. S.: Mathematical
778 Modelling of Arctic Polygonal Tundra with *Ecosys:* 2. Microtopography
779 Determines How CO_2 and CH_4 Exchange Responds to Changes in Temperature
780 and Precipitation: GHG Exchange in Arctic Polygonal Tundra, Journal of
781 Geophysical Research: Biogeosciences, 122(12), 3174–3187,
782 doi:10.1002/2017JG004037, 2017b.
783 Guo, D., Wang, H. and Wang, A.: Sensitivity of Historical Simulation of the Permafrost
784 to Different Atmospheric Forcing Data Sets from 1979 to 2009, Journal of
785 Geophysical Research: Atmospheres, 122(22), 12,269-12,284,
786 doi:10.1002/2017JD027477, 2017.
787 Harris, I., Jones, P. D., Osborn, T. J. and Lister, D. H.: Updated high-resolution grids of
788 monthly climatic observations – the CRU TS3.10 Dataset, International Journal of
789 Climatology, 34(3), 623–642, doi:10.1002/joc.3711, n.d.

Hodgkins, S. B., Tfaily, M. M., McCalley, C. K., Logan, T. A., Crill, P. M., Saleska, S. R., Rich, V. I. and Chanton, J. P.: Changes in peat chemistry associated with permafrost thaw increase greenhouse gas production, Proceedings of the National Academy of Sciences, 111(16), 5819–5824, doi:10.1073/pnas.1314641111, 2014.

van den Hurk, B., Kim, H., Krinner, G., Seneviratne, S. I., Derksen, C., Oki, T., Douville, H., Colin, J., Ducharne, A., Cheruy, F., Viovy, N., Puma, M. J., Wada, Y., Li, W., Jia, B., Alessandri, A., Lawrence, D. M., Weedon, G. P., Ellis, R., Hagemann, S., Mao, J., Flanner, M. G., Zampieri, M., Materia, S., Law, R. M. and Sheffield, J.: LS3MIP (v1.0) contribution to CMIP6: the Land Surface, Snow and Soil moisture Model Intercomparison Project – aims, setup and expected outcome, Geoscientific Model Development, 9(8), 2809–2832, doi:10.5194/gmd-9-2809-2016, 2016.

Hugelius, G., Strauss, J., Zubrzycki, S., Harden, J. W., Schuur, E. A. G., Ping, C.-L., Schirrmeister, L., Grosse, G., Michaelson, G. J., Koven, C. D., O'Donnell, J. A., Elberling, B., Mishra, U., Camill, P., Yu, Z., Palmtag, J. and Kuhry, P.: Estimated stocks of circumpolar permafrost carbon with quantified uncertainty ranges and identified data gaps, Biogeosciences, 11(23), 6573–6593, doi:10.5194/bg-11-6573-2014, 2014.

IPCC, 2014: Climate Change 2014: Synthesis Report. Contribution of Working Groups I, II and III to the Fifth Assessment Report of the Intergovernmental Panel on Climate Change [Core Writing Team, R.K. Pachauri and L.A. Meyer (eds.)]. IPCC, Geneva, Switzerland, 151 pp.

812 Johansson, M., Callaghan, T. V., Bosiö, J., Åkerman, H. J., Jackowicz-Korczynski, M.
813 and Christensen, T. R.: Rapid responses of permafrost and vegetation to
814 experimentally increased snow cover in sub-arctic Sweden, Environmental
815 Research Letters, 8(3), 035025, doi:10.1088/1748-9326/8/3/035025, 2013.
816 Johansson, T., Malmer, N., Crill, P. M., Friborg, T., åKerman, J. H., Mastepanov, M. and
817 Christensen, T. R.: Decadal vegetation changes in a northern peatland, greenhouse
818 gas fluxes and net radiative forcing, Global Change Biology, 12(12), 2352–2369,
819 doi:10.1111/j.1365-2486.2006.01267.x, 2006.
820 Jones, M. C., Harden, J., O'Donnell, J., Manies, K., Jorgenson, T., Treat, C. and Ewing,
821 S.: Rapid carbon loss and slow recovery following permafrost thaw in boreal
822 peatlands, Glob. Chang. Biol., 23(3), 1109–1127, doi:10.1111/gcb.13403, 2017.
823 Kalnay, E., Kanamitsu, M., Kistler, R., Collins, W., Deaven, D., Gandin, L., Iredell, M.,
824 Saha, S., White, G., Woollen, J., Zhu, Y., Chelliah, M., Ebisuzaki, W., Higgins,
825 W., Janowiak, J., Mo, K. C., Ropelewski, C., Wang, J., Leetmaa, A., Reynolds,
826 R., Jenne, R. and Joseph, D.: The NCEP/NCAR 40-Year Reanalysis Project, Bull.
827 Amer. Meteor. Soc., 77(3), 437–472, doi:10.1175/1520-
828 0477(1996)077<0437:TNYRP>2.0.CO;2, 1996.
829 Kanamitsu, M., Ebisuzaki, W., Woollen, J., Yang, S.-K., Hnilo, J. J., Fiorino, M. and
830 Potter, G. L.: NCEP–DOE AMIP-II Reanalysis (R-2), Bull. Amer. Meteor. Soc.,
831 83(11), 1631–1644, doi:10.1175/BAMS-83-11-1631, 2002.
832 Kokfelt, U., Reuss, N., Struyf, E., Sonesson, M., Rundgren, M., Skog, G., Rosen, P., and
833 Hammarlund, D.: Wetland development, permafrost history and nutrient cycling

inferred from late Holocene peat and lake sediment records in subarctic Sweden, J. Paleolimn., 44, 327–342, doi:10.1007/s10933-010-9406- 8, 2010.

Lundin, E. J., Klaminder, J., Giesler, R., Persson, A., Olefeldt, D., Heliasz, M., Christensen, T. R. and Karlsson, J.: Is the subarctic landscape still a carbon sink? Evidence from a detailed catchment balance, Geophysical Research Letters, 43(5), 1988–1995, doi:10.1002/2015GL066970, 2016.

Malmer, N., Johansson, T., Olsrud, M. and Christensen, T. R.: Vegetation, climatic changes and net carbon sequestration in a North-Scandinavian subarctic mire over 30 years, Global Change Biology, 11(11), 1895–1909, doi:10.1111/j.1365-2486.2005.01042.x, 2005.

Mastepanov, M., Sigsgaard, C., Dlugokencky, E. J., Houweling, S., Ström, L., Tamstorf, M. P. and Christensen, T. R.: Large tundra methane burst during onset of freezing, Nature, 456(7222), 628–630, doi:10.1038/nature07464, 2008.

McCalley, C. K., Woodcroft, B. J., Hodgkins, S. B., Wehr, R. A., Kim, E.-H., Mondav, R., Crill, P. M., Chanton, J. P., Rich, V. I., Tyson, G. W. and Saleska, S. R.: Methane dynamics regulated by microbial community response to permafrost thaw, Nature, 514(7523), 478–481, doi:10.1038/nature13798, 2014.

Mezbahuddin, M., Grant, R. F. and Hirano, T.: Modelling effects of seasonal variation in water table depth on net ecosystem CO_2 exchange of a tropical peatland, Biogeosciences, 11(3), 577–599, doi:10.5194/bg-11-577-2014, 2014.

Mondav, R., McCalley, C. K., Hodgkins, S. B., Frolking, S., Saleska, S. R., Rich, V. I., Chanton, J. P. and Crill, P. M.: Microbial network, phylogenetic diversity and community membership in the active layer across a permafrost thaw gradient,

857 Environmental Microbiology, 19(8), 3201–3218, doi:10.1111/1462-2920.13809,
858 2017.
859 Mondav, R., Woodcroft, B. J., Kim, E.-H., McCalley, C. K., Hodgkins, S. B., Crill, P.
860 M., Chanton, J., Hurst, G. B., VerBerkmoes, N. C., Saleska, S. R., Hugenholtz, P.,
861 Rich, V. I. and Tyson, G. W.: Discovery of a novel methanogen prevalent in
862 thawing permafrost, Nature Communications, 5, 3212, doi:10.1038/ncomms4212,
863 2014.
864 Myhre, G., D. Shindell, F.-M. Bréon, W. Collins, J. Fuglestvedt, J. Huang, D. Koch, J.-F.
865 Lamarque, D. Lee, B. Mendoza, T. Nakajima, A. Robock, G. Stephens, T.
866 Takemura and H. Zhang, 2013: Anthropogenic and Natural Radiative Forcing. In:
867 Climate Change 2013: The Physical Science Basis. Contribution of Working
868 Group I to the Fifth Assessment Report of the Intergovernmental Panel on
869 Climate Change [Stocker, T.F., D. Qin, G.-K. Plattner, M. Tignor, S.K. Allen, J.
870 Boschung, A. Nauels, Y. Xia, V. Bex and P.M. Midgley (eds.)]. Cambridge
871 University Press, Cambridge, United Kingdom and New York, NY, USA, pp.
872 659–740, doi:10.1017/ CBO9781107415324.018.
873 O'Donnell, J. A., Jorgenson, M. T., Harden, J. W., McGuire, A. D., Kanevskiy, M. Z. and
874 Wickland, K. P.: The Effects of Permafrost Thaw on Soil Hydrologic, Thermal,
875 and Carbon Dynamics in an Alaskan Peatland, Ecosystems, 15(2), 213–229,
876 doi:10.1007/s10021-011-9504-0, 2012.
877 Olefeldt, D. and Roulet, N. T.: Effects of permafrost and hydrology on the composition
878 and transport of dissolved organic carbon in a subarctic peatland complex, Journal

of Geophysical Research: Biogeosciences, 117(G1), doi:10.1029/2011JG001819, 2012.

Piao, S., Liu, Z., Wang, T., Peng, S., Ciais, P., Huang, M., Ahlstrom, A., Burkhart, J. F., Chevallier, F., Janssens, I. A., Jeong, S.-J., Lin, X., Mao, J., Miller, J., Mohammat, A., Myneni, R. B., Peñuelas, J., Shi, X., Stohl, A., Yao, Y., Zhu, Z. and Tans, P. P.: Weakening temperature control on the interannual variations of spring carbon uptake across northern lands, Nature Climate Change, 7(5), 359–363, doi:10.1038/nclimate3277, 2017.

Raz-Yaseef, N., Torn, M. S., Wu, Y., Billesbach, D. P., Liljedahl, A. K., Kneafsey, T. J., Romanovsky, V. E., Cook, D. R. and Wullschleger, S. D.: Large CO2 and CH4 emissions from polygonal tundra during spring thaw in northern Alaska, Geophysical Research Letters, 44(1), 504–513, doi:10.1002/2016GL071220, 2017.

Rydén, B. E., Fors, L. and Kostov, L.: Physical Properties of the Tundra Soil-Water System at Stordalen, Abisko, Ecological Bulletins, (30), 27–54, 1980.

Schuur, E. a. G., McGuire, A. D., Schädel, C., Grosse, G., Harden, J. W., Hayes, D. J., Hugelius, G., Koven, C. D., Kuhry, P., Lawrence, D. M., Natali, S. M., Olefeldt, D., Romanovsky, V. E., Schaefer, K., Turetsky, M. R., Treat, C. C. and Vonk, J. E.: Climate change and the permafrost carbon feedback, Nature, 520(7546), 171–179, doi:10.1038/nature14338, 2015.

Sonesson, M. (1972) Cryptogams. In: International biological programme—Swedish tundra biome project. Technical report No. 9, April 1972. Swedish Natural Science Research Council Ecological Research Committee.

902 Tokida, T., Miyazaki, T., Mizoguchi, M., Nagata, O., Takakai, F., Kagemoto, A. and
903 Hatano, R.: Falling atmospheric pressure as a trigger for methane ebullition from
904 peatland, Global Biogeochemical Cycles, 21(2), doi:10.1029/2006GB002790,
905 2007.
906 Viovy, N.: CRUNCEP Version 7 - Atmospheric Forcing Data for the Community Land
907 Model, Research Data Archive at the National Center for Atmospheric Research,
908 Computational and Information Systems Laboratory, Boulder CO.
909 Wickland, K. P., Striegl, R. G., Neff, J. C. and Sachs, T.: Effects of permafrost melting
910 on CO2 and CH4 exchange of a poorly drained black spruce lowland, Journal of
911 Geophysical Research: Biogeosciences, 111(G2), doi:10.1029/2005JG000099,
912 2006.
913 Woodcroft, B. J., Singleton, C. M., Boyd, J. A., Evans, P. N., Emerson, J. B., Zayed, A.
914 A. F., Hoelzle, R. D., Lamberton, T. O., McCalley, C. K., Hodgkins, S. B.,
915 Wilson, R. M., Purvine, S. O., Nicora, C. D., Li, C., Frolking, S., Chanton, J. P.,
916 Crill, P. M., Saleska, S. R., Rich, V. I. and Tyson, G. W.: Genome-centric view of
917 carbon processing in thawing permafrost, Nature, doi:10.1038/s41586-018-0338-
918 1, 2018.
919 Wu, Z., Ahlström, A., Smith, B., Ardö, J., Eklundh, L., Fensholt, R. and Lehsten, V.:
920 Climate data induced uncertainty in model-based estimations of terrestrial
921 primary productivity, Environmental Research Letters, 12(6), 064013,
922 doi:10.1088/1748-9326/aa6fd8, 2017.

923 Yoshimura, K. and Kanamitsu, M.: Dynamical Global Downscaling of Global
924 Reanalysis, Monthly Weather Review, 136(8), 2983–2998,
925 doi:10.1175/2008MWR2281.1, 2008.
926 Zaehle, S., Friend, A. D., Friedlingstein, P., Dentener, F., Peylin, P. and Schulz, M.:
927 Carbon and nitrogen cycle dynamics in the O-CN land surface model: 2. Role of
928 the nitrogen cycle in the historical terrestrial carbon balance, Global
929 Biogeochemical Cycles, 24(1), doi:10.1029/2009GB003522, 2010.
930 Zimov, S. A., Davydov, S. P., Zimova, G. M., Davydova, A. I., Schuur, E. a. G., Dutta,
931 K. and Chapin, F. S.: Permafrost carbon: Stock and decomposability of a globally
932 significant carbon pool, Geophysical Research Letters, 33(20),
933 doi:10.1029/2006GL027484, 2006.
934

935 Table 1. Temporal coverage of quality-controlled CO_2 and CH_4 exchanges measured by
936 automated chambers at the three peatland types in the Stordalen Mire during the years
937 2002 to 2007.

	CO_2			CH_4		
Sites	Number of data points	3 Hourly coverage (%)	Daily coverage (%)	Number of data points	3 Hourly coverage (%)	Daily coverage (%)
Palsa	12752	65.8	12.4	N/A	N/A	N/A
Bog	12821	68.5	12.7	6660	96.2	25.0
Fen	8989	63.8	13.7	4923	90.5	33.7

938

939 Table 2. Evaluation of the 3 hourly and daily CO_2 and CH_4 exchanges simulated at the

940 palsa, bog, and fen sites. RRMSEs are relative root mean squared errors.

		3-Hourly		Daily	
		R^2	RRMSEs (%)	R^2	RRMSEs (%)
Sites	C component				
Palsa	CO_2	0.48	13.4	0.36	18.3
Bog	CO_2	0.63	19.1	0.44	35.8
	CH_4	0.31	16.3	0.47	22.3
Fen	CO_2	0.64	8.4	0.43	25.5
	CH_4	0.44	11.1	0.54	16.9

941

942

943 Table 3. Means and standard deviations of cumulative CO_2 and CH_4 exchanges simulated

944 in the palsa, bog, and fen during the period 2003 to 2007. All exchanges are in units of g

945 C m^{-2}.

		Growing season; Days 119–288		Non-growing season; Days 1–118/289–365	
		Mean	Standard deviation	Mean	Standard deviation
Sites	C flux component				
Palsa					
	CO_2	-72.70	19.10	38.89	4.09
	CH_4	0.04	0.02	0.01	0.002
Bog					
	CO_2	-79.59	21.46	42.89	2.16
	CH_4	3.52	0.45	0.42	0.11
Fen					
	CO_2	-88.65	7.26	44.41	6.13
	CH_4	10.86	3.95	0.78	0.18

946

947

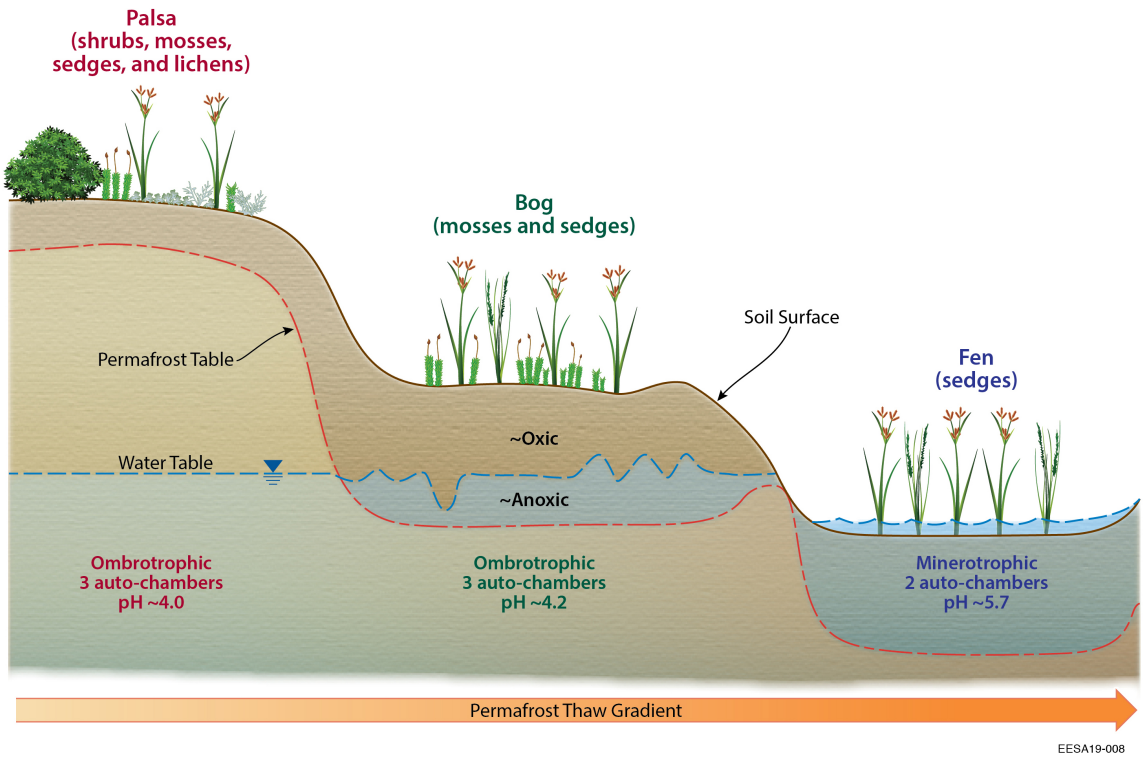

948

949 Figure 1. Schematic diagram of the sampling sites at Stordalen Mire.

950

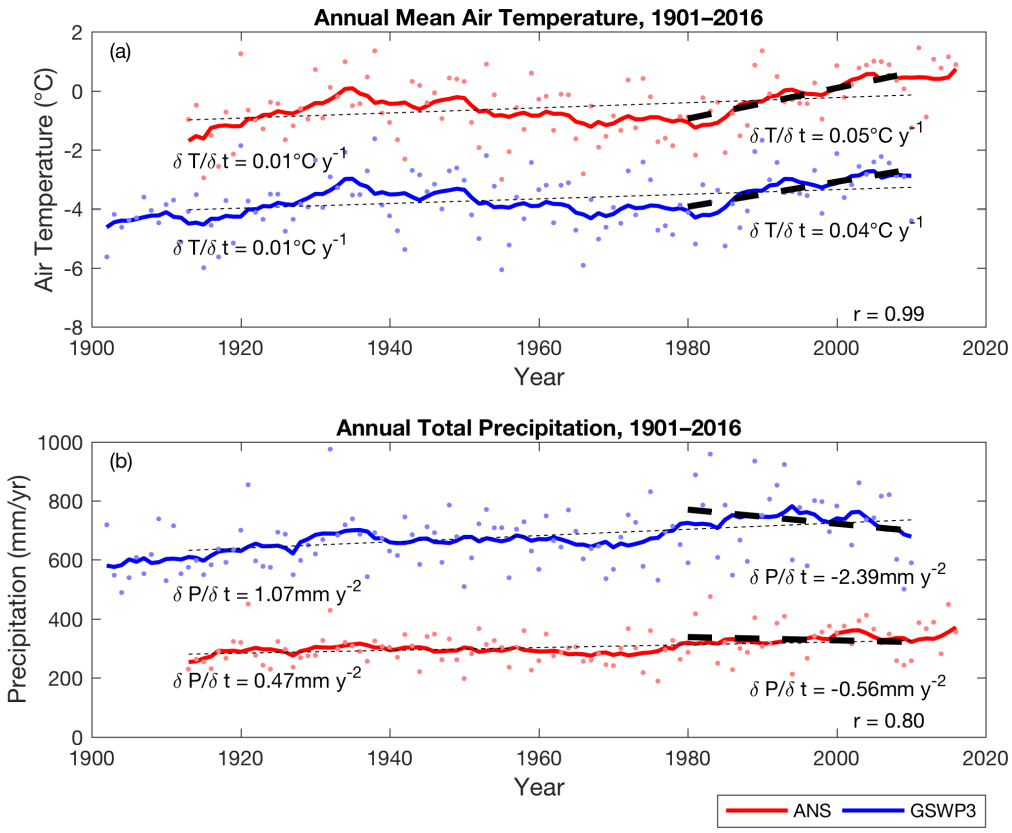

951

952 Figure 2. Time series of air temperature (a) and precipitation (b) measured at ANS (red;
953 years 1913–2016) and extracted from GSWP3 (blue; years 1901–2010). Dots are the
954 annual means and solid lines are the decadal moving averages of the corresponding
955 annual means. Thin and thick dashed lines are the trends for years 1913–2010, and years
956 1980–2010, respectively. The inset r values are the correlation coefficients calculated
957 between the two time series.

958

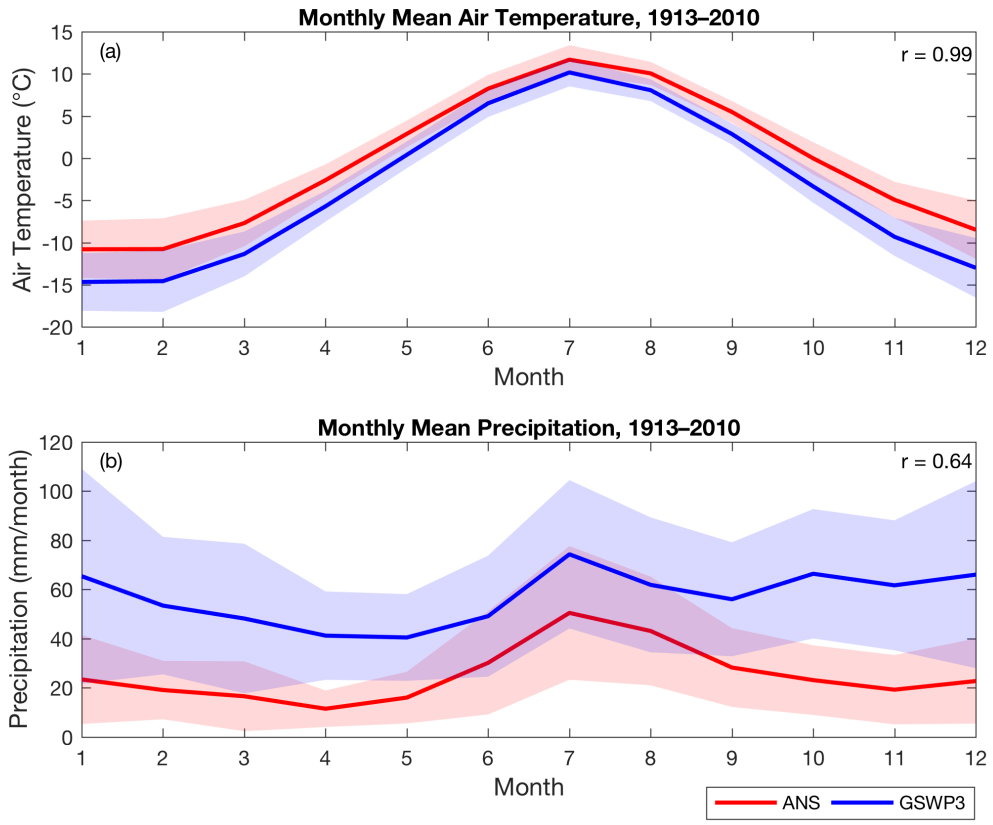

Figure 3. Monthly mean air temperature (a) and precipitation (b) measured at ANS (red) and extracted from GSWP3 (blue). The shaded area is the inter-annual variability for the corresponding dataset, represented by the standard deviations calculated at each month. The inset r values are the correlation coefficients calculated between the two time series.

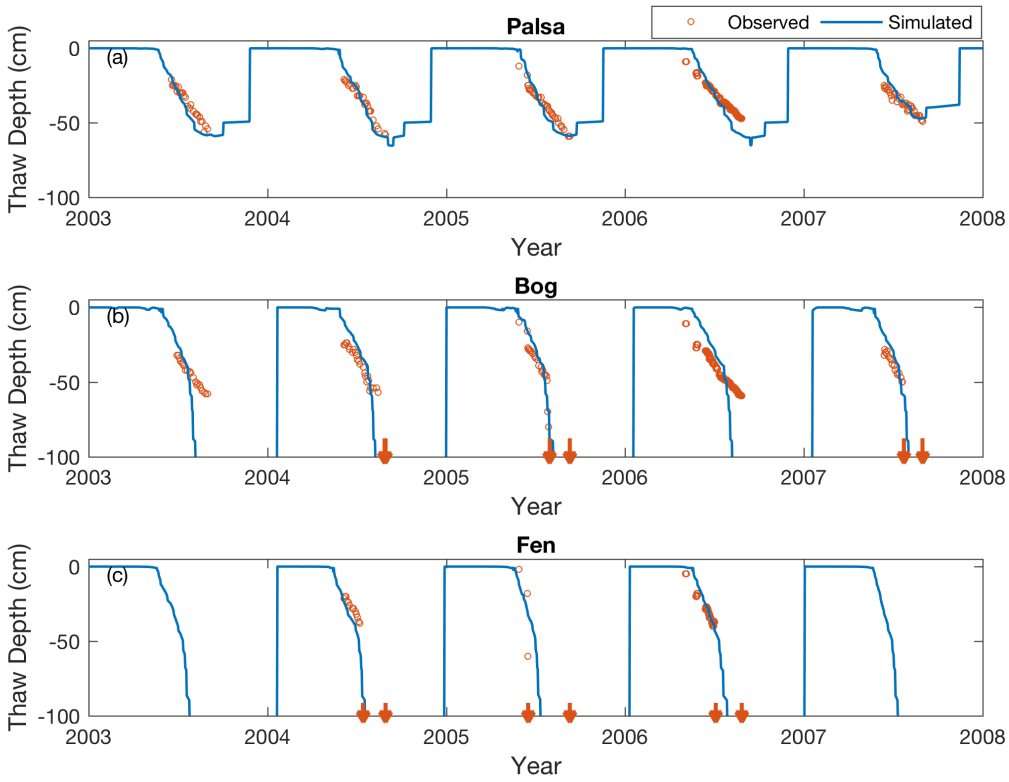

965

966 Figure 4. Simulated (solid lines) and measured (open circles) seasonal dynamics of thaw

967 depth at the palsa (a), bog (b), and fen (c) sites from 2003 to 2007. Downward arrows

968 indicate the time when measured thaw depth deepens below 90 cm for a measurement

969 year.

970

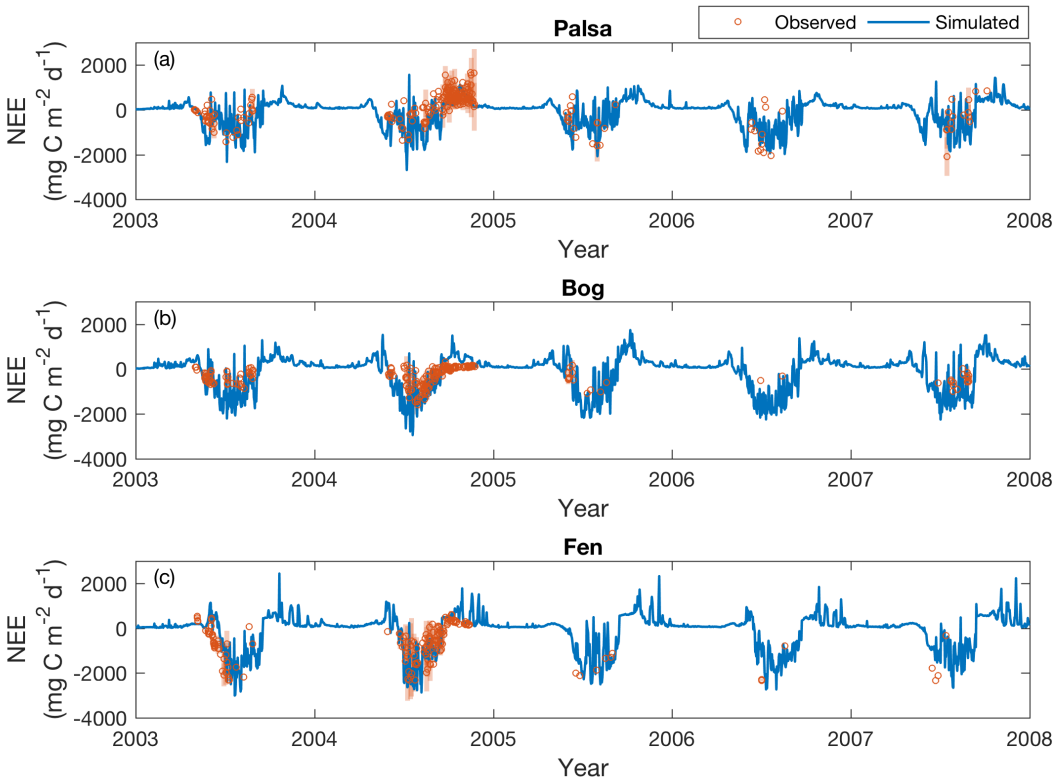

971

972 Figure 5. Simulated (solid lines) and measured (open circles) daily CO_2 exchanges (NEE)

973 at the palsa (a), bog (b), and fen (c) sites, from 2003 to 2007. Shaded bars are the

974 standard deviations of daily NEE measured across subsites under each peatland type.

975 Positive and negative values indicate effluxes from and influxes to the site, respectively.

976

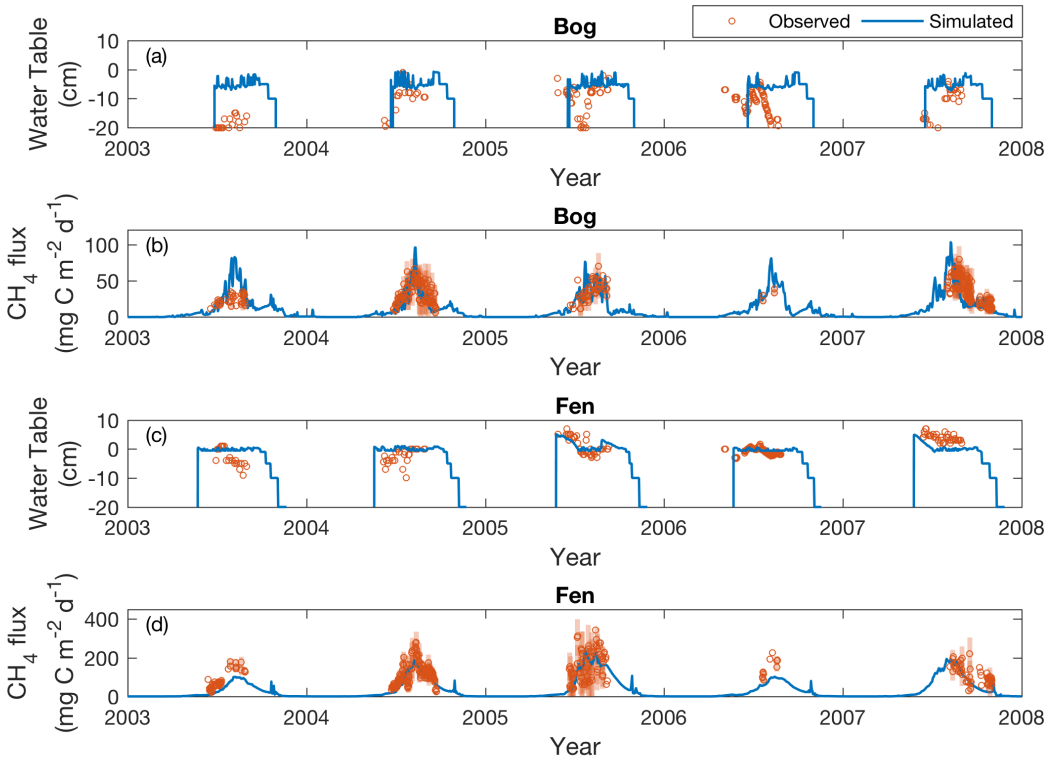

977

978 Figure 6. Simulated (solid lines) and measured (open circles) water table depth and daily

979 CH_4 emissions at the bog and fen from 2003 to 2007. Shaded bars are the standard

980 deviations of the daily CH_4 emissions measured across the subsites under each peatland

981 type.

982

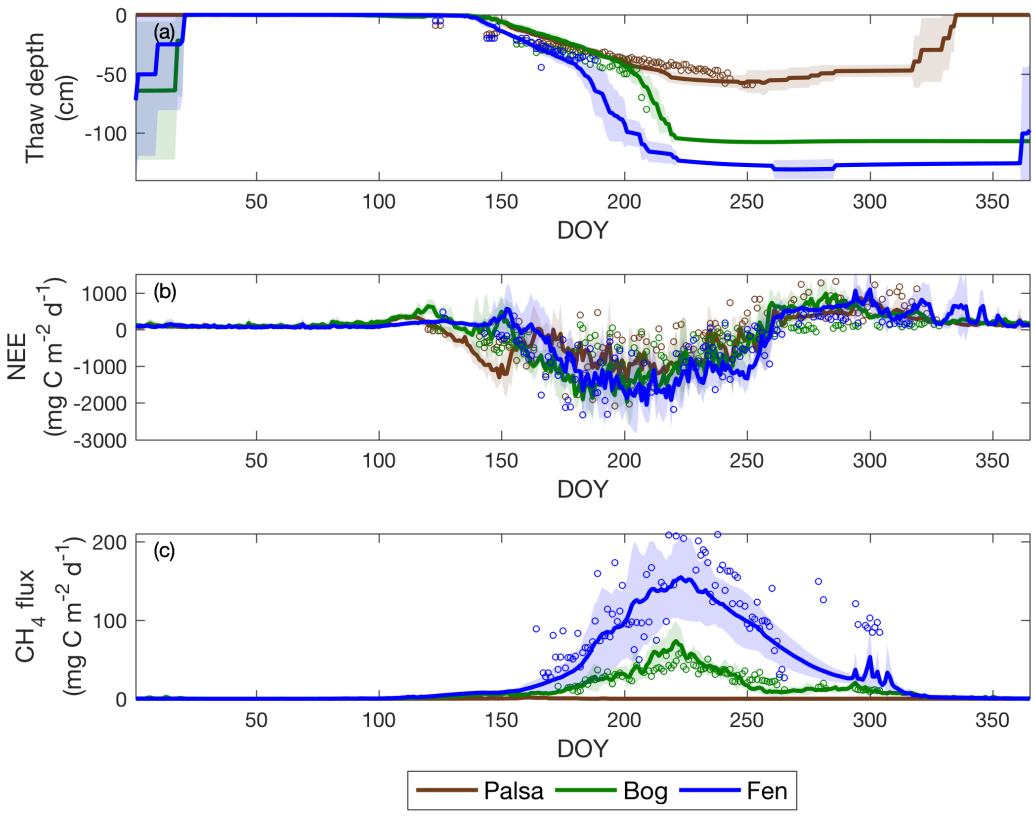

983

984 Figure 7. Daily thaw depth (a), daily NEE (b), and daily CH_4 (c) exchanges for the three

985 sites from 2003 to 2007. Solid lines and open circles are the simulated and measured

986 inter-annual means for each day of year, respectively. The shaded area is the simulated

987 inter-annual variability for the corresponding dataset, represented by the standard

988 deviations calculated at each day of year. Positive and negative carbon flux values

989 indicate effluxes from and influxes to the site, respectively.

990

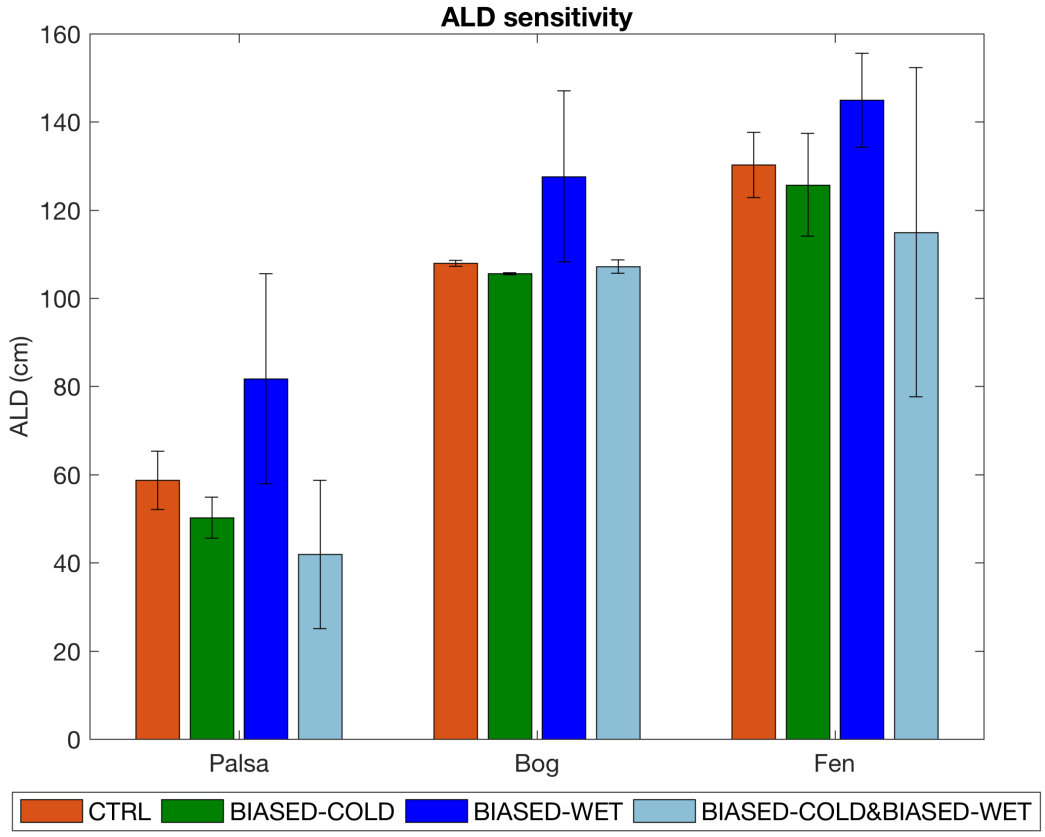

Figure 8. Simulated ALD at the palsa, bog, and fen for four sets of climate forcing (Section 2.5). Bars and error bars are means and standard deviations calculated from 2003 to 2007, respectively.

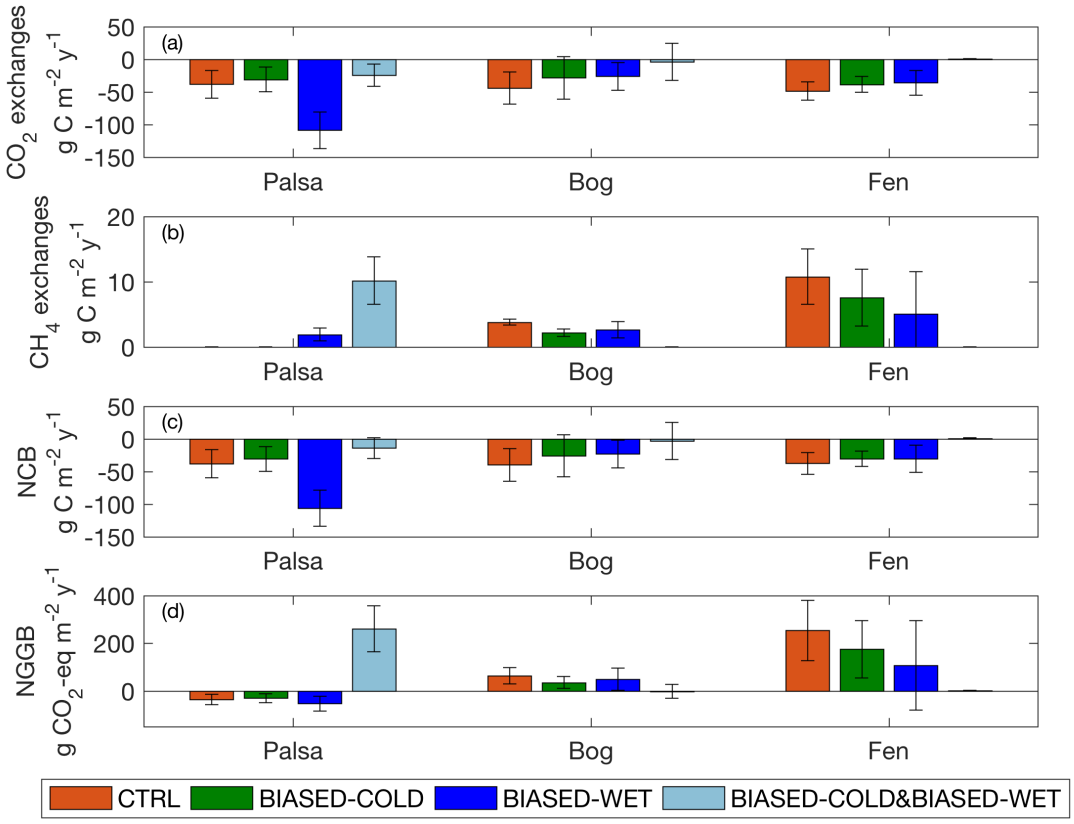

997

998 Figure 9. Annual CO_2 exchanges (a), CH_4 exchanges (b), Net Carbon Balance (c), and

999 Net Greenhouse Gas Balance (d) simulated at the palsa, bog, and fen, under each set of

1000 simulations. Bars and error bars are the means and standard deviations calculated from

1001 2003 to 2007, respectively. Positive and negative values indicate effluxes from and

1002 influxes to the site, respectively.

1003

1004